ECRONICON OPEN ACCESS

EC PHARMACOLOGY AND TOXICOLOGY
Research Article

Phosphatidylinositol 4,5-Diphosphate Inhibits Interaction of Cobra Venom Cytotoxin with Model Lipid Membranes: Pharmacological Relevance

Shuhao Zhang[1], Ziqin Wang[1], Yuri N Utkin[2], Ruben K Dagda[3] and Edward S Gasanoff[1,4]*

[1]*Advanced STEM Research Center, Chaoyang Kaiwen Academy, Beijing, China*

[2]*Shemyakin-Ovchinnikov Institute of Bioorganic Chemistry, Russian Academy of Sciences, Moscow, Russia*

[3]*Department of Pharmacology, University of Nevada Medical School, Reno, NV, USA*

[4]*Belozersky Institute of Physico-Chemical Biology, M.V. Lomonosov Moscow State University, Moscow, Russia*

***Corresponding Author:** Edward S Gasanoff, Advanced STEM Research Center, Chaoyang Kaiwen Academy, Beijing, China.

Received: February 25, 2026; **Published:** March 18, 2026

DOI: 10.31080/ECPT.2026.14.00955

Abstract

The role of phosphatidylinositol and its phosphorylated derivatives-present at low levels in the plasma membranes of most cells but abundant in membranes of brain cells-remains poorly understood. In this study, we employed differential scanning calorimetry and AutoDock docking simulations to investigate whether phosphatidylinositol and its phosphoinositide derivatives may protect nerve cell membranes from attack by amyloidogenic proteins. To model amyloidogenic proteins, we used cobra venom cytotoxin CTII, which exhibits membranotropic properties similar to those of amyloidogenic proteins.

Our results demonstrate that cytotoxin CTII significantly disrupts the packing order of phosphatidylinositol in model membranes. However, phosphorylation of phosphatidylinositol appears to protect membranes from CTII insertion. A single phosphate group (PI-3-PO_4^{2-}) markedly attenuates CTII's disruptive effect on the packing of lipid bilayers, while two phosphate groups (PI-4,5-PO_4^{2-}) completely prevent membrane insertion and disruption. In the latter case, CTII is instead anchored at the membrane surface, promoting tighter lipid packing. If confirmed in future studies, these findings could inform the development of novel pharmaceuticals that protect cell membranes from attack by membrane-active protein toxins with amyloidogenic-like properties. Additionally, these findings suggest that phosphorylated derivatives of phosphatidylinositol may play a protective role in nerve cell membranes against amyloidogenic proteins.

Keywords: *Phosphatidylinositol 4,5-Diphosphate; Cobra Venom Cytotoxin; Lipid Membranes*

Abbreviations

PI: Phosphatidylinositol; PI-3-PO_4^{2-}: Phosphatidylinositol 3-Phosphate (PI-3-PO_4^{2-}); PI-4,5-PO_4^{2-}: Phosphatidylinositol 4,5-Diphosphate; DSC: Differential Scanning Calorimetry; SCM: Solution for Calorimetric Measurements

Introduction

Phosphatidylinositol (PI) is a distinctive phospholipid featuring a cyclohexane ring, known as inositol, linked to the phosphate group within its polar head [1]. Although present in membranes of all cell types at relatively lower concentrations compared to other phospholipids, PI is particularly enriched in brain tissue, where it accounts for up to 10% of the total phospholipid content [1]. PI can also be phosphorylated to form phosphoinositides by Phosphoinositide 3-kinases kinases, with one or two phosphate groups attached to

specific carbon atoms of the inositol ring. Among the most prevalent phosphoinositides are PI-3-PO_4^{2-}, which has a phosphate at the third carbon, and PI-4,5-PO_4^{2-}, which contains phosphates at the fourth and fifth carbons [2-4]. While the structural and functional contributions of PI and phosphoinositides are not yet completely understood, accumulating evidence implicates them in essential cellular activities, including membrane trafficking, signal transduction, and autophagy in eukaryotic cells. Nevertheless, the precise molecular details of these processes and the distinct functions of individual phosphoinositides remain to be fully elucidated [5,6].

Outside of brain tissue, phosphoinositides are generally found at low levels, representing roughly 0.5 - 1% of the total lipids in the inner leaflet of the plasma membrane. Existing data indicate that PI does not likely play a dominant structural role under normal physiological conditions [1]. However, during malignant development, an increase in the concentration of PI-diphosphates has been observed in the outer leaflet of the plasma membrane [7], and during the progression of Alzheimer's disease, elevated levels of PI-di- and triphosphates have been detected in the membranes of endosomes and lysosomes [8]. These findings suggest a potential connection to disease resistance [1]. Despite PI and phosphoinositides already being abundant in membranes of brain cells, their concentrations may experience a transient rise in the early phases of neurological disorders, implying a protective function against disease progression [1], possibly by inhibiting the interaction and aggregation of amyloidogenic proteins within nerve cell membranes [9,10].

Cytotoxin CTII, also referred to as cardiotoxin, is a low-molecular-mass (approximately 7 kDa) cationic protein isolated from the venom of cobra *Naja oxiana* [11]. This protein binds to various membrane phospholipids [12,13] and, at low concentrations, mimics the behavior of membrane-active proteins found in cytosol involved in modulating membrane permeability and fusion [13]. Cytotoxin CTII also affects proton transport through the F_0 subunit of ATP synthase [14,15] and alters membrane signaling [12] by influencing the packing arrangement of phospholipids [11,16]. Cytotoxin CTII has been proposed as a model protein for studying the membranotropic properties of amyloidogenic proteins and their interactions with nerve cell membranes [10,11]. Additionally, cytotoxin CTII has been extensively employed in investigations which modeled native membranotropic cellular and extracellular proteins using artificial membranes with varying phospholipid compositions [10-16]. However, the interaction of CTII with phosphatidylinositol and its phosphorylated derivatives has not been examined to date.

The objective of this study was to determine whether the presence of phosphate groups on the inositol ring of phosphatidylinositol influences the interaction between cytotoxin CTII and lipid membranes, with the overall goal of exploring the potential inhibitory effect of these phosphate groups on CTII binding to lipid membrane. As an initial step, we examined how the incorporation of phosphate groups into the inositol ring affects the packing of PI within lipid membranes. Subsequently, we assessed whether CTII differentially alters the lipid packing order in membranes composed of PI, PI-3-PO_4^{2-}, or PI-4,5-PO_4^{2-}. For these experiments, we employed Differential Scanning Microcalorimetry (DSMC), a method that allows precise measurement of two key physical parameters: the enthalpy change (kJ/mol) and the transition temperature (T °C) associated with the shift of saturated lipid membranes from a solid crystalline state to a liquid-gel phase [17]. These parameters define the shape of the calorimetric curves obtained during lipid melting, offering valuable information on the lipid packing order in saturated membranes [17].

Furthermore, we investigated whether the presence and positional arrangement of phosphate groups on the inositol ring affect intermolecular bonding and the binding sites of PI on the CTII molecular surface. To address this, we utilized AutoDock Vina Version 4.2, a leading computational tool for analyzing biomolecular interactions.

By correlating the observed differences in lipid packing order in membranes containing PI and its phosphorylated derivatives-both in the absence and presence of CTII-with variations in binding sites and intermolecular bonds between PI (and its derivatives) and CTII, we aimed to gain deeper insight into the functional roles of PI and its derivatives within cellular membranes. The results of this study suggest that a phosphate group on the inositol ring of phosphatidylinositol plays a key role in inhibiting CTII penetration into the membrane, by sterically binding to CTII in an unproductive manner. This novel insight holds promise for the development of new pharmaceutical strategies aimed at preventing neurological disorders linked to the aberrant interaction of proteins with nerve cell membranes.

Materials and Methods

Materials

Synthetic phospholipids of 98% purity were obtained from BOS Sciences (Shirley, NY, USA): dipalmitoyl phosphatidylinositol (PI), dipalmitoyl phosphatidylinositol 3-phosphate (PI-3-PO_4^{2-}), and dipalmitoyl phosphatidylinositol 4,5-diphosphate (PI-4,5-PO_4^{2-}). Cytotoxin CTII (99% purity) was isolated from *Naja oxiana* cobra venom following a previously described procedure [18]. EDTA (99.5% purity) and 0.1 mol/L Tris-HCl buffer (pH 7.4) were purchased from Thermo Fisher Scientific Inc. (Waltham, MA, USA). Methanol (≥ 99.8% purity) and chloroform (≥ 99.8% purity) were obtained from Merck KGaA (Darmstadt, Germany). Deionized distilled water (ddH_2O) was sourced from XiZhiMeng Co., Ltd. (Guangdong, China).

Equipment

The equipment used in this study included DASM-4 Differential Scanning Microcalorimeter (Saint-Petersburg, Russia) equipped with the program converting heat (kJ) released by mole of phospholipid to enthalpy change (kJ/mol), Vacuum Pump TW-1M (Tingwei Co. Ltd., Wenling, China), High Precision Balance FA2004 (Shanghai Maiyi Ltd. Co., China), Digital Water Thermostat SHHW.21-420 (YongGuangMing Medical Instrument Ltd. Co., Beijing, China), PC HYLR-WFQ9 with installed Auto-Dock Vina Version 4.2 and MGL Tools Python Molecular Viewer (Scripps Research Institute) programs, Eppendorf plastic vials and Hamilton 100 microliter (μdm^3) syringe (Hamilton Co., Boston, USA).

Preparation of stock solutions

To prepare 0.03 mol/L stock solutions of each phospholipid, 243.3 mg of PI, 267.3 mg of PI-3-PO_4^{2-}, and 291.3 mg of PI-4,5-PO_4^{2-} were weighed. Each phospholipid was placed in a separate 10 mL volumetric flask and dissolved in a methanol : chloroform mixture (1:1, v/v) to a final volume of 10 mL.

A buffer solution for calorimetric measurements (SCM) was prepared containing 0.1M Tris-HCl (pH 7.4), 0.1M NaCl, 0.1 mM $CaCl_2$, and 5 mM EDTA. To prepare 100 mL of this buffer, I weighed 0.585g of NaCl, 11.1 mg of $CaCl_2$, and 116.9 mg of EDTA, placed them in a 100 mL volumetric flask, and added 0.1M Tris-HCl (pH 7.4) to a final volume of 100 mL.

A 1.5×10^{-4}M CTII stock solution was prepared by weighing 10.5 mg of CTII into a 10 mL volumetric flask and dissolving it in SCM buffer to a final volume of 10 mL.

Preparation of phospholipid dispersions

For calorimetric measurements, 100 μL of each phospholipid stock solution was placed into separate vacuum tubes. The methanol and chloroform were removed by vacuum drying at room temperature for two hours. The resulting phospholipid film was then hydrated with 1.0 mL of SCM buffer at 63°C in a thermostat (SHHW.21-420). For samples treated with CTII, 100 μL of CTII stock solution was added to the vacuum tube containing the phospholipid film, followed by 900 μL of SCM buffer. All phospholipid dispersions-both with and without CTII-were vortexed for 30 minutes at 63°C, then incubated for three hours in the thermostat at 63°C. This temperature is above the phase transition from the solid crystalline to the liquid-gel state.

Differential scanning microcalorimetry (DSC)

Calorimetric curves of phospholipid dispersions, both in the absence and presence of CTII, were recorded using a DASM-4 differential scanning microcalorimeter at a scan rate of 1°C/min. An initial calibration scan with distilled water was performed at 50 mW with $\Delta T = 4$ to establish the instrumental baseline. For each experimental condition, phospholipid dispersion samples with or without CTII were tested in triplicate. Each reported ΔH (kJ/mol) and transition temperature (T °C) value represents the mean of three independent trials.

Molecular docking simulations

To identify potential binding sites for PI, PI-3-PO_4^{2-}, and PI-4,5-PO_4^{2-} on the molecular surface of CTII, docking simulations were performed using AutoDock Vina (version 4.2) [19]. The atomic coordinates for CTII were obtained from the Protein Data Bank (PDB code: 1CB9). The three-dimensional structures of PI, PI-3-PO_4^{2-}, and PI-4,5-PO_4^{2-} were constructed in PDB format using ChemDraw and Chem3D software. Energy minimization and charge verification were carried out using GROMOS force fields prior to docking. All molecules were hydrated at pH 7.4 using the hydration function in AutoDock. A blind docking approach was employed to scan the entire molecular surface of CTII. The grid box was defined with the following parameters: center coordinates (x = -0.836, y = 3.125, z = 0.929) and box dimensions (size x = 33.75, size y = 34.50, size z = 36.75). The CTII molecule was treated as rigid, while all phospholipid ligands were allowed full rotational freedom. Each CTII-phospholipid pair was docked in triplicate. No variation in intermolecular bond sets or overall binding geometry was observed across replicate runs for any docking pair. Intermolecular interactions-including hydrogen bonds, ion-polar contacts, and ionic bonds-were analyzed using the MGL Tools Python Molecular Viewer (Scripps Research Institute).

Uncertainties

- 100 ml volumetric flask ± 0.10000 ml: (0.10000 ml / 100 ml) × 100% = 0.10000%.
- 10 ml volumetric flask ± 0.01000 ml: (0.0100 ml / 10 ml) × 100% = 0.10000%.
- 100 µl Hamilton syringe: (0.1000 µl / 100 µl) × 100% = 0.10000%.
- High precision balance ± 0.00010g: (0.00010 g / 0.58500 g) × 100% = 0.01709%.
- High precision balance ± 0.00010g: (0.00010 g / 0.01050 g) × 100% = 0.95238%.
- Digital thermometer (± 0.0500°C): (0.0500°C / 50.0000°C) × 100% = 0.10000%.
- DSMC apparatus (± 0.010 kJ/mol): (0.010 kJ/mol/29.103 kJ/mol) × 100% = 0.03436%.
- Total uncertainty: 1.40383%.

Safety measures and ethical considerations

Methanol is lethal if ingested and toxic when inhaled [20]. Chloroform is harmful upon contact with skin or eyes and is carcinogenic if ingested [21]. CTII is hazardous if it enters the bloodstream. To ensure safety throughout the experiments, protective goggles, rubber gloves, and a laboratory coat were worn at all times. All procedures involving chloroform and methanol were conducted under a fume hood. Hazardous chemical waste was collected in designated plastic containers for disposal by the environmental safety department. No ethical concerns were associated with this study.

Statistical analysis

For each enthalpy change (ΔH) data point, the standard deviation (SD) within triplicate test runs never exceeded 3% of the mean. Student's t-test was used to compare ΔH values between samples with and without CTII. Additionally, one-way ANOVA was employed to assess statistical differences in ΔH values among the three sample types-PI, PI-3-PO_4^{2-}, and PI-4,5-PO_4^{2-}-both in the presence and absence of CTII. A *p*-value of less than 0.05 was considered statistically significant. No statistical analysis was performed for transition temperature (T °C), as no variation was observed among triplicate samples for any data point. Similarly, statistical analysis was not conducted for the AutoDock docking study, as no variation was detected across triplicate runs for each docking pair.

Results and Analysis

DSC study

The three-dimensional structure of cobra venom cytotoxin CTII consists of antiparallel β-strands that form three hydrophobic loops, flanked by cationic lysine and arginine residues [20]. This structural arrangement facilitates CTII's interaction with membranes

composed of anionic phospholipids. The hydrophobic loops interact with phospholipid alkyl chains via London dispersion forces, while the cationic residues form ionic bonds with the polar head groups of phospholipids. Consequently, the long molecular axes of CTII and the phospholipids align parallel to one another and perpendicular to the membrane surface [20], as illustrated in figure 1. While the interaction of CTII with anionic phospholipids have been extensively studied including cardiolipin, the interaction of CTII with membranes composed of PI has not yet been reported. However, given that PI is an anionic phospholipid, its mode of interaction with CTII is expected to follow the same pattern depicted in figure 1.

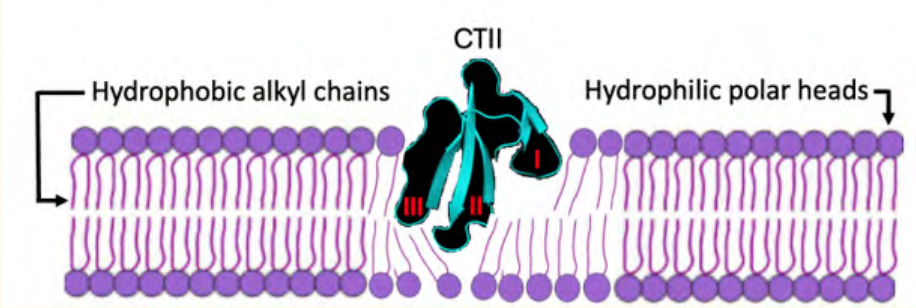

Figure 1: *Interaction of cobra venom cytotoxin CTII with a model membrane of anionic phospholipids. CTII consists of three hydrophobic loops-designated I, II, and III-formed by antiparallel β-strands. This structural arrangement, in which hydrophobic loops are flanked by cationic lysine (Lys) and arginine (Arg) residues, drives the interaction of CTII with the membrane. The hydrophobic loops insert into the lipid bilayer, forming non-polar intermolecular bonds with the alkyl chains, while the cationic residues form ionic bonds with the polar head groups of anionic phospholipids [22]. The bilayer membrane shown above is adapted from [23], and the three-dimensional structure of CTII was obtained from the Protein Data Bank (PDB code: 1CB9).*

Insertion of CTII into a PI membrane, with its long axis aligned parallel to that of PI, would disrupt the packing order of PI within the bilayer, as illustrated in figure 1. This disturbance is expected to alter the thermodynamic properties of the membrane. To investigate whether CTII disrupts lipid packing by penetrating membranes composed of PI, PI-3-PO_4^{2-}, and PI-4,5-PO_4^{2-}, we employed differential scanning microcalorimetry (DSC).

The calorimetric curve shape for the phase transition of saturated lipids from a solid crystalline to a liquid-gel state reflects the degree of lipid packing order within the membrane. A highly ordered packing of saturated phospholipids is characterized by a narrow main transition peak and a small pretransition peak occurring approximately 10°C below the main transition temperature as previously reported by others [22]. Disruption of lipid packing eliminates the pretransition peak, broadens the main transition peak, and reduces its height. Additionally, such disturbances lead to a decrease in both the enthalpy change (ΔH) and the phase transition temperature (T_m), as less heat energy is required to induce the transition when lipid packing is less ordered [22].

The calorimetric curve of lipid bilayers comprising predominantly of PI exhibited a narrow main transition peak at 60.0°C and a distinct pretransition peak (Figure 2A), indicating a high degree of PI packing order within the membrane. In contrast, the calorimetric curves of samples composed of PI-3-PO_4^{2-} (Figure 1B) and PI-4,5-PO_4^{2-} (Figure 2C) lacked pretransition peaks and displayed broader main transition peaks at 58.0°C and 55.0°C, respectively. The enthalpy changes at phase transitions (Table 1) decreased progressively with an increasing number of phosphate groups on the inositol ring, demonstrating that additional phosphate groups reduce the phospholipid packing order within the membrane.

The addition of CTII to phospholipid dispersions composed of PI resulted in a significant broadening of the main transition peak and the complete elimination of the pretransition peak (Figure 2D). Both the enthalpy changes and transition temperature (Table 1) consequently decreased, indicating a reduction in phospholipid packing order triggered by the insertion of CTII into the PI membrane.

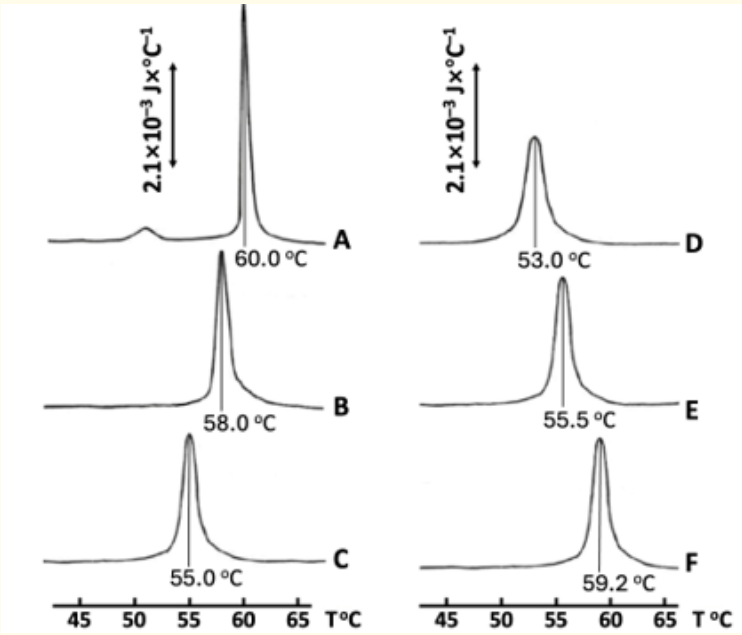

Figure 2: *Calorimetric curves of multilamellar phospholipid dispersions. Thermograms are shown for dispersions composed of: (A) 1,2-dipalmitoyl-sn-glycero-3-phosphatidylinositol (PI); (B) 1,2-dipalmitoyl-sn-glycero-3-phosphatidylinositol 3-phosphate (PI-3-PO_4); (C) 1,2-dipalmitoyl phosphatidylinositol 4,5-diphosphate (PI-4,5-PO_4); (D) PI in the presence of cardiotoxin CTII; (E) PI-3-PO_4 in the presence of CTII; and (F) PI-4,5-PO_4 in the presence of CTII. The phospholipid concentration in all samples was 3 mM. In samples containing CTII (D-F), the toxin concentration was 1.5 × 10^{-5} M. For each data point, samples were prepared in triplicate, and thermograms were recorded for each sample. No variation in transition temperature (T °C) or in the shape of the thermograms was observed across triplicate experimental trials for any data point.*

Multilamellar dispersions	$\Delta H/\Delta H_0^{\dagger}$ kJ/mol	Mean kJ/mol	SD	T °C	$\Delta H/\Delta H_0^{\ddagger}$ kJ/mol	Mean kJ/mol	SD	T °C	Student's p-values
PI	1.001 1.000 0.999	1.000	8.16×10^{-4}	60.0	0.730 0.732 0.731	0.731	8.15×10^{-4}	53.0	5.09×10^{-10}
PI-3-PO_4^{2-}	0.901 0.899 0.900	0.900	8.15×10^{-4}	58.0	0.873 0.870 0.870	0.871	1.41×10^{-3}	55.5	1.49×10^{-5}

PI-4,5-PO_4^{2-}	0.851 0.851 0.848	0.850	1.41×10^{-3}	55.0	0.943 0.942 0.941	0.942	8.16×10^{-4}	59.2	1.49×10^{-7}
ANOVA p-values	2.33×10^{-11}				3.02×10^{-12}				

Table 1: *Effects of phosphate groups at positions 3 and 4,5 of the inositol ring of 1,2-dipalmitoyl-sn-glycero-3-phosphatidylinositol (PI) on the enthalpy change (ΔH) and transition temperature (T °C) of the main phase transition peak of multilamellar phospholipid dispersions (PI, PI-3-PO_4^{2-}, or PI-4,5-PO_4^{2-}) in the absence (ΔH/ΔH$_0$†) and presence (ΔH/ΔH$_0$‡) of cytotoxin CTII. Phospholipid and CTII concentrations were 3 mM and 1.5 × 10^{-5}M, respectively. No variation in T °C was observed across triplicate experimental trials for any data point.*

ΔH/ΔH$_0$†, where ΔH$_0$† is the enthalpy change of multilamellar PI dispersions, and ΔH is the enthalpy change of multilamellar dispersions of PI, PI-3-PO_4^{2-}, or PI-4,5-PO_4^{2-} in the absence of CTII.

ΔH/ΔH$_0$‡, where ΔH$_0$‡ is the enthalpy change of multilamellar PI dispersions, and ΔH is the enthalpy change of multilamellar dispersions of PI, PI-3-PO_4^{2-}, or PI-4,5-PO_4^{2-} in the presence of CTII.

The addition of CTII to phospholipid dispersions composed of PI-3-PO_4^{2-} resulted in a slight broadening of the main transition peak (Figure 2E) compared to the PI-3-PO_4^{2-} sample in the absence of CTII. The enthalpy change of the main transition peak showed an insignificant decrease, while the transition temperature decreased by only 2.5°C (Table 1). These observations indicate a minor reduction in phospholipid packing order, suggesting that only a limited number of CTII molecules are able to penetrate the PI-3-PO_4^{2-} membrane.

In contrast, the addition of CTII to phospholipid dispersions composed of PI-4,5-PO_4^{2-} produced no noticeable change in the width of the main transition peak (Figure 2F). However, both the enthalpy change and transition temperature increased (Table 1), indicating an enhancement in phospholipid packing order. This finding strongly suggests that CTII molecules do not penetrate the PI-4,5-PO_4^{2-} membrane.

Taken together, the DSC results indicate that an increasing number of phosphate groups on the inositol ring progressively hinders the ability of CTII to penetrate membranes composed of PI and its phosphorylated derivatives.

AutoDock study

To complement the DSC study, we employed AutoDock software to examine whether the interaction between CTII and PI results in the alignment of their long axes parallel to one another, thereby facilitating perpendicular insertion of CTII into the membrane. Additionally, we investigated whether phosphorylation of PI with one or two phosphate groups interferes with this steric arrangement of CTII with phosphorylated PI species, which promotes CTII insertion.

The binding sites, binding affinities (kJ/mol), and intermolecular interactions-including ionic, polar-ionic, and hydrogen bonds-between PI and CTII are summarized in table 2. The polar and charged groups of PI are labeled in figure 2.

Notably, the intermolecular interactions at binding sites 3, 5, and 7 were identical, with only minor variations in the binding of alkyl chains on the CTII surface. These variations did not affect the overall binding geometry of the PI-CTII complex. For simplicity, therefore, binding sites 5 and 7 were omitted from table 2, and only binding site 3 is presented.

Number of binding site and binding affinity	Type of bond	Charged and polar groups of polar head of PI	Charged and polar groups of CTII
#1 -16.7 (kJ/mol)	Polar-ionic Polar-ionic Polar-ionic Polar-ionic Polar-ionic Hydrogen	1-$PO^{\delta-}$C 6-$O^{\delta-}$H 4-$O^{\delta-}$H 5-$O^{\delta-}$H II-C=$O^{\delta-}$ 2-$CO^{\delta-}$C	Lys5($N^{+}H_3$) Lys5($N^{+}H_3$) Lys18($N^{+}H_3$) Lys18($N^{+}H_3$) Lys35($N^{+}H_3$) Tyr22($OH^{\delta+}$)
#2 -16.7 (kJ/mol)	Hydrogen Polar-ionic Polar-ionic	3-$O^{\delta-}$H 4-$O^{\delta-}$H 6-$O^{\delta-}$H	Cys38($NH_{pb}^{\delta+}$) Lys5($N^{+}H_3$) Lys18($N^{+}H_3$)
#3 -16.7 (kJ/mol)	Ionic Polar-ionic Polar-ionic Polar-ionic Polar-ionic Hydrogen	PO_4^- PO_4^- 2-$O^{\delta-}$H 3-$O^{\delta-}$H II-C=$O^{\delta-}$ 2-$CO^{\delta-}$C	Lys5($N^{+}H_3$) Cys38($NH_{pb}^{\delta+}$) Lys18($N^{+}H_3$) Lys18($N^{+}H_3$) Lys35($N^{+}H_3$) Tyr22($OH^{\delta+}$)
#4 -16.7 (kJ/mol)	Ion-polar Ion-polar	3-$O^{\delta-}$H 5-$O^{\delta-}$H	Lys18($N^{+}H_3$) Lys5($N^{+}H_3$)
#6 -15.9 (kJ/mol)	Hydrogen Hydrogen Hydrogen	I-C=$O^{\delta-}$ II-C=$O^{\delta-}$ 3-$OH^{\delta+}$	Cys53($NH_{pb}^{\delta+}$) Ser45($OH^{\delta+}$) Asn($CO^{\delta-}$)
#8 -15.9 (kJ/mol)	Hydrogen Hydrogen	I-C=$O^{\delta-}$ 2-$CO^{\delta-}$C	Cys53($NH_{pb}^{\delta+}$) Ser45($OH^{\delta+}$)
#9 -15.5 (kJ/mol)	Ionic Polar-ionic Polar-ionic Polar-ionic Polar-ionic	PO_4^- II-C=$O^{\delta-}$ I-C=$O^{\delta-}$ 1-$CO^{\delta-}$C 2-$CO^{\delta-}$C	Lys18($N^{+}H_3$) Lys18($N^{+}H_3$) Lys12($N^{+}H_3$) Lys5($N^{+}H_3$) Lys5($N^{+}H_3$)

Table 2: *Binding affinities (kJ/mol) and intermolecular interactions between the polar head groups of PI and the polar and charged groups of CTII amino acid residues, as determined by AutoDock Vina (Version 4.2) docking simulations. "Pb" in $NH_{pb}^{\delta+}$ denotes a peptide bond. The polar and charged groups of the PI polar head are labeled in figure 2.*

Notably, in six of the docked conformations (binding sites 2, 3, 5, 6, 7, and 8), PI binds to hydrophobic loop III of CTII, with the long axes of both molecules aligned parallel to one another. This binding mode is illustrated in figure 3, which shows the CTII-PI interaction in both surface representation (A) and lines-cartoon-sticks representation (B). These findings suggest that CTII inserts into the PI membrane with its long axis oriented perpendicular to the membrane surface.

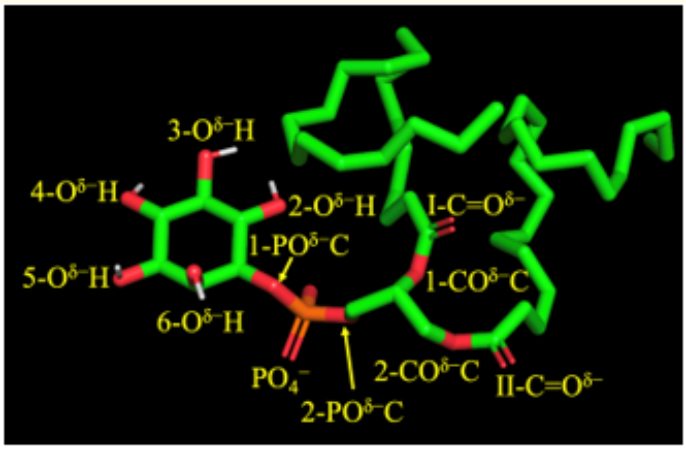

Figure 3: *Notation of charged and polar groups on the polar head of phosphatidylinositol (PI). Atom color code: carbon - green, oxygen - red, phosphorus - orange, hydrogen - white.*

Table 3 summarizes the binding sites, binding affinities (kJ/mol), and intermolecular bonds-including ion-polar, ionic, and hydrogen bonds-identified in the nine docked conformations of PI-3-PO_4^{2-} with CTII. The charged and polar groups of PI-3-PO_4^{2-} are labeled in figure 4. Notably, none of the binding sites listed in Table 3 exhibit intermolecular bonds identical to those observed in table 2, which entailed the results of the docked structures of CTII with PI. These findings suggests that phosphorylation of the inositol ring at the carbon 3 position significantly alters the pattern of intermolecular bonding between PI and CTII.

Number of binding site and binding affinity	**Type of bond**	**Charged and polar groups of polar head of PI-3-PO_4^{2-}**	**Charged and polar groups of CTII**
#1 -15.9 (kJ/mol)	Polar-ionic Polar-ionic Polar-ionic Ionic	2-O$^{\delta-}$H 1-CO$^{\delta-}$C 2-CO$^{\delta-}$C 3-PO_4^{2-}	Lys23(-N$^+$H$_3$) Lys23(-N$^+$H$_3$) Lys23(-N$^+$H$_3$) His31(C$_3$N$^+$H)
#2 -15.5 (kJ/mol)	Ionic Polar-ionic Hydrogen Hydrogen Ion-polar	PO_4^- II-C=O$^{\delta-}$ 2-OH$^{\delta+}$ 2-O$^{\delta-}$H 3-PO_4^{2-}	His31(C$_3$N$^+$H) Lys23(N$^+$H$_3$) Asn60(CO$^{\delta-}$) Arg36(CNH$^{\delta+}$C) Arg36(-H$^{\delta+}$NH$^{\delta+}$)
#3 -15.1 (kJ/mol)	Ionic Hydrogen Polar-ionic Polar-ionic	PO_4^- 6-OH$^{\delta+}$ I-C=O$^{\delta-}$ II-C=O$^{\delta-}$	Lys5(-N$^+$H$_3$) Asn60(CO$^{\delta-}$) Lys23(-N$^+$H$_3$) Lys23(-N$^+$H$_3$)

#4 -15.1 (kJ/mol)	Polar-ionic Hydrogen Ionic Polar-ionic	3-PO_4^{2-} 2-$O^{\delta-}$H PO_4^- 1-$PO^{\delta-}$C	Arg36(-$H^{\delta+}NH^{\delta+}$) Arg36($CNH^{\delta+}$C) Lys23(-N^+H_3) Lys23(-N^+H_3)
#5 -14.6 (kJ/mol)	Hydrogen Hydrogen Hydrogen	5-$OH^{\delta+}$ 5-$O^{\delta-}$H II-C=$O^{\delta-}$	Leu6(C=$O_{pb}^{\delta-}$) Arg36(-$H^{\delta+}NH^{\delta+}$) Arg36(-$H^{\delta+}NH^{\delta+}$)
#6 -14.6 (kJ/mol)	Ionic Polar-ionic Polar-ionic Polar-ionic Polar-ionic Hydrogen Hydrogen	3-PO_4^{2-} 3-PO_4^{2-} 2-$O^{\delta-}$H I-C=$O^{\delta-}$ 1-$CO^{\delta-}$C 6-$OH^{\delta+}$ 5-$OH^{\delta+}$	His31(C_3N^+H) His31(C=$O_{pb}^{\delta-}$) Lys23(-N^+H_3) Lys23(-N^+H_3) Lys23(-N^+H_3) Cys59(C=$O_{pb}^{\delta-}$) Asn60($CO^{\delta-}$)
#7 -14.6 (kJ/mol)	Hydrogen Hydrogen Hydrogen	5-$O^{\delta-}$H I-C=$O^{\delta-}$ 6-$OH^{\delta+}$	Arg36(-$H^{\delta+}NH^{\delta+}$) Arg36(-$H^{\delta+}NH^{\delta+}$) Pro33(C=$O_{pb}^{\delta-}$)
#8 -14.6 (kJ/mol)	Polar-ionic Polar-ionic Polar-ionic	1-$PO^{\delta-}$C 2-$O^{\delta-}$H 2-$CO^{\delta-}$C	Lys23(N^+H_3) Lys23(N^+H_3) Lys23(N^+H_3)
#9 -14.6 (kJ/mol)	Polar-ionic Polar-ionic Polar-ionic Polar-ionic Hydrogen	5-$O^{\delta-}$H 6-$O^{\delta-}$H 1-$CO^{\delta-}$C II-C=$O^{\delta-}$ 6-$O^{\delta-}$H	Lys23(N^+H_3) Lys23(N^+H_3) Lys23(N^+H_3) Lys23(N^+H_3) Arg36($CNH^{\delta+}$C)

Table 3: *Binding affinities (kJ/mol) and intermolecular bonds between the polar head groups of PI-3-PO_4^{2-} and the polar and charged groups of CTII amino acid residues, as determined by AutoDock Vina (Version 4.2) docking simulations. The polar and charged groups of the PI-3-PO_4^{2-} polar head are labeled in figure 4. "Pb" in C=$O_{pb}^{\delta-}$ denotes a peptide bond.*

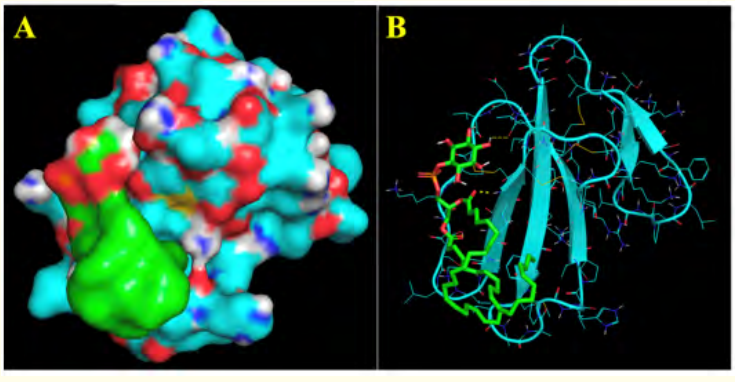

Figure 4: *Interaction of PI with CTII at binding site 6 (See table 2). (A) Molecular surface representation: CTII surface is shown with the following atom color code: carbon - emerald, oxygen - red, hydrogen - white, nitrogen - blue, sulfur - yellow. PI surface follows the same color code, except carbon is shown in green. (B) Combined cartoon and stick representation: CTII is depicted as a cartoon (emerald) with side chains shown as lines using the same atom color code as in (A). PI is shown as sticks with the same atom color code as in (A), except carbon is green. Yellow dashed lines indicate intermolecular bonds.*

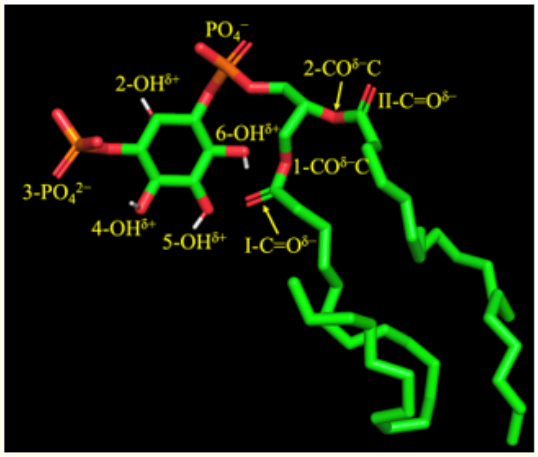

Figure 5: *Notation of charged and polar groups on the polar head of phosphatidylinositol-3-phosphate (PI-3-PO42-). Atom color code: carbon - green, oxygen - red, phosphorus - orange, hydrogen - white.*

Analysis of the docked conformations of PI-3-PO_4^{2-} with CTII did not reveal binding to the hydrophobic loops of CTII with parallel alignment of their long axes. Instead, PI-3-PO_4^{2-} was found to bind to the hydrophobic loops of CTII with its long axis oriented perpendicular to that of CTII, as illustrated in figure 6. This binding orientation suggests that PI-3-PO_4^{2-} is unlikely to adopt such a conformation when incorporated into a bilayer membrane.

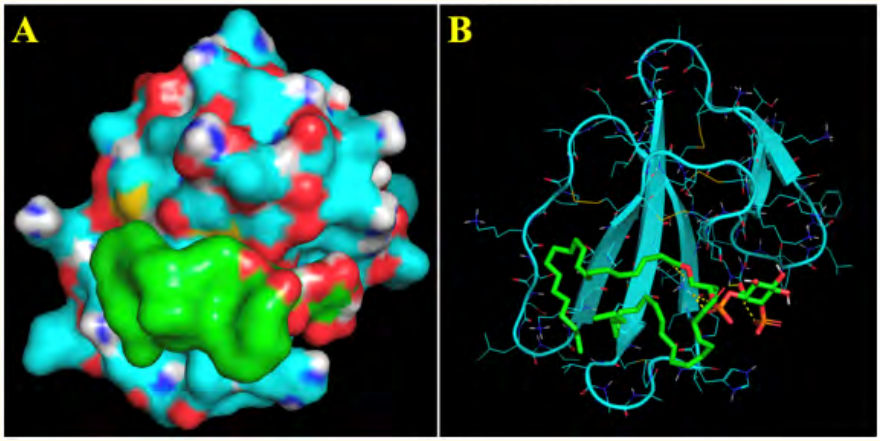

Figure 6: *Interaction of PI-3-PO4^{2-} with CTII at binding site 4 (See table 3). (A) Molecular surface representation: CTII surface is shown with the following atom color code: carbon - emerald, oxygen - red, hydrogen - white, nitrogen - blue, sulfur - yellow. PI-3-PO4^{2-} surface follows the same color code, except carbon is shown in green. (B) Combined cartoon and stick representation: CTII is depicted as a cartoon (emerald) with side chains shown as lines using the same atom color code as in (A). PI-3-PO4^{2-} is shown as sticks with the same atom color code as in (A), except carbon is green. Yellow dashed lines indicate intermolecular bonds.*

The binding sites, binding affinities, and intermolecular bonds-including ion-polar, ionic, and hydrogen bonds-between PI-4,5-PO_4^{2-} and CTII, as identified by AutoDock simulations, are shown in table 4. The polar and charged groups of PI-4,5-PO_4^{2-} are labeled in figure 7. For this pair of docked molecules, AutoDock identified identical sets of intermolecular bonds across four binding sites (1, 2, 3, and 6). Therefore, in table 4, site 1 is presented as representative of all four sites. Notably, the conformations of PI, PI-3-PO_4^{2-}, and PI-4,5-PO_4^{2-} when docked with CTII differ markedly in their binding sites and intermolecular bond patterns.

Number of binding site and binding affinity	Type of bond	Charged and polar groups of polar head of PI-4,5-PO_4^{2-}	Charged and polar groups of CTII
#1 -18.4 (kJ/mol)	Ionic Ionic Polar-ionic Ionic Ionic Ionic Polar-ionic Polar-ionic Hydrogen Polar-ionic Hydrogen	5-PO_4^{2-} 5-PO_4^{2-} 6-$O^{\delta-}$H PO_4^- 4-PO_4^{2-} 3-$O^{\delta-}$H 2-$O^{\delta-}$H 1-P$O^{\delta-}$C II-C=$O^{\delta-}$ 2-C$O^{\delta-}$C	Lys12(-N^+H_3) Lys5(-N^+H_3) Lys5(-N^+H_3) Lys5(-N^+H_3) Lys18(-N^+H_3) Lys18(-N^+H_3) Lys18(-N^+H_3) Cys38($NH_{pb}^{\delta+}$) Lys35(-N^+H_3) Tyr22($OH^{\delta+}$)
#4 -18.0 (kJ/mol)	Ionic Ionic Polar-ionic Ionic Ionic Polar-ionic Hydrogen	5-PO_4^{2-} 5-PO_4^{2-} 6-$O^{\delta-}$H PO_4^- 4-PO_4^{2-} 2-$O^{\delta-}$H 1-P$O^{\delta-}$C	Lys12(-N^+H_3) Lys5(-N^+H_3) Lys5(-N^+H_3) Lys5(-N^+H_3) Lys18(-N^+H_3) Lys18(-N^+H_3) Cys38($NH_{pb}^{\delta+}$)
#5 -17.6 (kJ/mol)	Ionic Ionic Polar-ionic Ionic Polar-ionic	5-PO_4^{2-} 5-PO_4^{2-} 6-$O^{\delta-}$H 4-PO_4^{2-} II-C=$O^{\delta-}$	Lys12(-N^+H_3) Lys5(-N^+H_3) Lys5(-N^+H_3) Lys18(-N^+H_3) Lys35(-N^+H_3)
#7 -17.6 (kJ/mol)	Ionic Ionic Ionic Polar-ionic Hydrogen	5-PO_4^{2-} 5-PO_4^{2-} 4-PO_4^{2-} 2-$O^{\delta-}$H 6-$O^{\delta-}$H	Lys12(-N^+H_3) Lys5(-N^+H_3) Lys18(-N^+H_3) Lys18(-N^+H_3) Cys38($NH_{pb}^{\delta+}$)
#8 -16.7 (kJ/mol)	Polar-ionic Ionic Polar-ionic	4-PO_4^{2-} 5-PO_4^{2-} 2-C$O^{\delta-}$C	Arg36(-$H^{\delta+}NH^{\delta+}$) Lys23(N^+H_3) Lys23(N^+H_3)
#9 -16.3 (kJ/mol)	Ionic Ionic Polar-ionic Polar-ionic Polar-ionic Polar-ionic Polar-ionic	5-PO_4^{2-} 5-PO_4^{2-} 6-$O^{\delta-}$H 2-C$O^{\delta-}$C I-C=$O^{\delta-}$ 2-$O^{\delta-}$H PO_4^-	Lys12(N^+H_3) Lys5(N^+H_3) Lys5(N^+H_3) Lys5(N^+H_3) Lys5(N^+H_3) Lys18(N^+H_3) Cys38($NH_{pb}^{\delta+}$)

Table 4: *Binding affinities (kJ/mol) and intermolecular bonds between the polar head groups of PI-4,5-PO_4^{2-} and the polar and charged groups of CTII amino acid residues, as determined by AutoDock Vina (Version 4.2) docking simulations. "Pb" in $NH_{pb}^{\delta+}$ denotes a peptide bond. The polar and charged groups of the PI-4,5-PO_4^{2-} polar head are labeled in figure 6.*

It should be noted that in eight of the nine binding sites, the polar head of PI-4,5-PO_4^{2-} bound to the CTII surface above the hydrophobic loops. This binding mode is stabilized by ionic bonds between the phosphate groups of PI-4,5-PO_4^{2-} and residues Lys5, Lys12, and Lys18 of CTII, as shown in table 4 and figure 7. Notably, only in binding site 8 (See table 4) did PI-4,5-PO_4^{2-} bind to the hydrophobic loops of CTII with its long axis oriented perpendicular to that of CTII, as illustrated in figure 8. Overall, the binding modes observed across all sites in table 4 and figure 7 and 8 are not conducive or productive for the insertion of CTII into the membrane. Therefore, we conclude that phosphorylation of the inositol ring interferes with CTII membrane insertion.

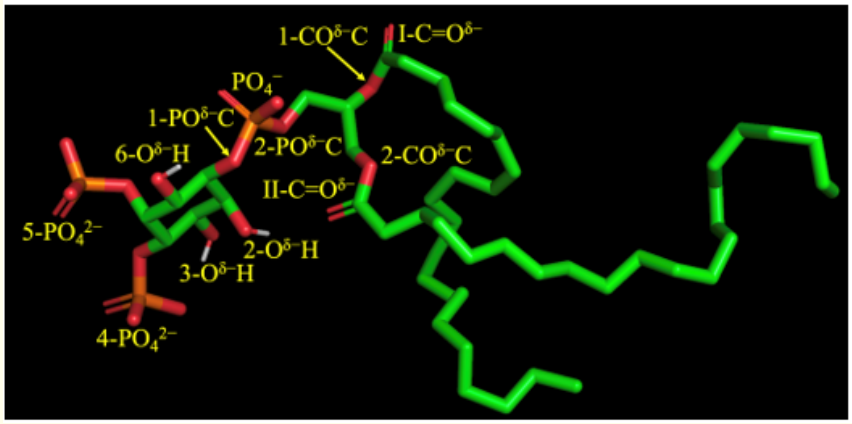

Figure 7: *Notation of charged and polar groups on the polar head of phosphatidylinositol 4,5-diphosphate (PI-4,5-$PO4^{2-}$). Atom color code: carbon - green, oxygen - red, phosphorus - orange, hydrogen - white.*

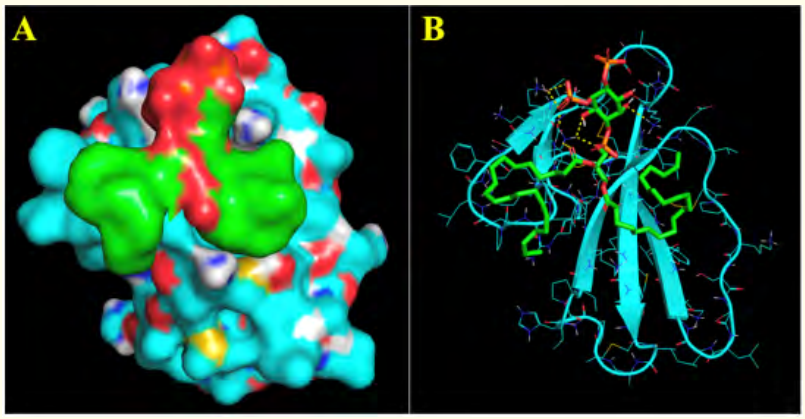

Figure 8: *Interaction of PI-4,5-$PO4^{2-}$ with CTII at binding site 9 (See table 4). (A) Molecular surface representation: CTII surface is shown with the following atom color code: carbon - emerald, oxygen - red, hydrogen - white, nitrogen - blue, sulfur - yellow. PI-4,5-$PO4^{2-}$ surface follows the same color code, except carbon is shown in green. (B) Combined cartoon and stick representation: CTII is depicted as a cartoon (emerald) with side chains shown as lines using the same atom color code as in (A). PI-4,5-$PO4^{2-}$ is shown as sticks with the same atom color code as in (A), except carbon is green. Yellow dashed lines indicate intermolecular bonds.*

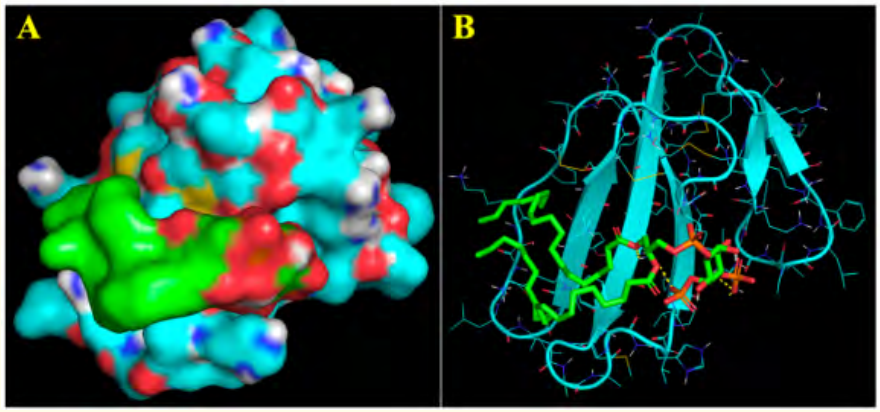

Figure 9: *Interaction of PI-4,5-PO4^{2-} with CTII at binding site 8 (See table 4). (A) Molecular surface representation: CTII surface is shown with the following atom color code: carbon - emerald, oxygen - red, hydrogen - white, nitrogen - blue, sulfur - yellow. PI-4,5-PO4^{2-} surface follows the same color code, except carbon is shown in green. (B) Combined cartoon and stick representation: CTII is depicted as a cartoon (emerald) with side chains shown as lines using the same atom color code as in (A). PI-4,5-PO4^{2-} is shown as sticks with the same atom color code as in (A), except carbon is green. Yellow dashed lines indicate intermolecular bonds.*

Discussion

It has been established that CTII penetrates membranes composed of anionic phospholipids, with its long molecular axis oriented perpendicular to the membrane surface and parallel to the long axis of the phospholipids [12]. Prior to this study, the interaction of CTII with membranes composed of phosphatidylinositol (PI) and its phosphorylated derivatives, PI-3-PO_4^{2-} and PI-4,5-PO_4^{2-}, had not been investigated.

Using differential scanning calorimetry (DSC), we observed that both the enthalpy change (ΔH) and the main transition temperature (T_m) decreased progressively across samples from PI to PI-3-PO_4^{2-} and PI-4,5-PO_4^{2-} (Table 1). This trend reflects a reduction in phospholipid packing order as the number of phosphate groups on the inositol ring increases. The additional phosphate groups likely enhance electrostatic repulsion between adjacent phospholipid head groups, thereby disrupting membrane packing.

The addition of CTII to PI dispersions disrupted the packing order of the membrane, as evidenced by decreases in both ΔH and T_m (Table 1). AutoDock simulations supported this observation, predicting that the long axis of PI aligns parallel to that of CTII-a configuration consistent with CTII inserting into the membrane with its long axis perpendicular to the membrane surface.

In contrast, CTII caused only minor disruption to PI-3-PO_4^{2-} membranes. The decreases in ΔH and T_m were negligible compared to PI-3-PO_4^{2-} samples without CTII (Table 1). Molecular surface analysis revealed that PI-3-PO_4^{2-} binds to the hydrophobic loops of CTII with its long axis oriented perpendicular to that of CTII (Figure 5). This binding mode is unfavorable for membrane insertion, suggesting that only a small fraction of CTII molecules may penetrate the membrane, resulting in minimal disruption of lipid packing.

Remarkably, the addition of CTII to PI-4,5-PO_4^{2-} membranes increased both ΔH and T_m relative to samples without CTII (Table 1), indicating enhanced phospholipid packing order. AutoDock studies revealed that the phosphate groups on the inositol ring of PI-4,5-PO_4^{2-} predominantly form ionic bonds with Lys5, Lys12, and Lys18 of CTII-residues located above the hydrophobic loops (Figure 7 and table

4). These ionic interactions neutralize the negative charge on the phosphates, reducing electrostatic repulsion between adjacent PI-4,5-PO_4^{2-} molecules and promoting tighter lipid packing. This mechanism accounts for the observed increase in ΔH and T_m upon CTII binding.

Given that lipid bilayers composed of PI-3-PO_4^{2-} or PI-4,5-PO_4^{2-} already exhibit disordered packing (Figure 2), one might predict that CTII would not significantly further reduce the packing of these membranes. Indeed, CTII is able to modestly reduce the packing of PI-3-PO_4^{2-} bilayers. In contrast, CTII noticeably increases the packing order of lipid bilayers composed of PI-4,5-PO_4^{2-} (Figure 2). Remarkably, both phosphorylated PI species directly inhibit the membrane-disruptive activity of CTII. They exhibit binding affinities (-16 to -18 kJ/mol) comparable to that of PI (-16 kJ/mol), yet they bind in a manner that is sterically non-productive and suboptimal for membrane insertion (Figures 6-9).

We acknowledge several limitations of this study. First, follow-up *in silico* studies using all-atom or coarse-grained molecular dynamics simulations would be valuable to further corroborate our initial AutoDock findings. Such simulations could model the interaction of CTII with virtual lipid bilayers composed of PI and its phosphorylated derivatives, providing deeper insight into the perpendicular binding orientation observed for PI-3-PO_4^{2-} and PI-4,5-PO_4^{2-}-an orientation that appears non-productive for membrane insertion.

Second, while PI-3-PO_4^{2-} and PI-4,5-PO_4^{2-} are the most abundant phosphoinositides, other species such as PI-3,4,5-PO_4^{2-} exist in much lower abundance in biological membranes. Future studies should investigate whether this tri-phosphorylated species similarly modulates CTII-membrane interactions.

Finally, it would be beneficial to explore whether other amyloidogenic proteins-both in monomeric and oligomeric forms-interact with PI-3-PO_4^{2-} and PI-4,5-PO_4^{2-} membranes. Proteins such as amyloid-beta and alpha-synuclein, which are implicated in the pathology of Alzheimer's and Parkinson's diseases respectively and are known to have high affinity for anionic lipids (e.g. cardiolipin and PI), may exhibit similar or distinct membrane-disruptive behaviors.

Conclusion and Implications

In summary, the number of phosphate groups on the inositol ring profoundly influences both the intrinsic packing of PI-derived membranes and their susceptibility to CTII. Increasing phosphorylation progressively reduces membrane packing order due to electrostatic repulsion. However, phosphorylation also appears to protect membranes from CTII-induced disruption and further disturbance of the overall organization of lipid bilayers. A single phosphate (PI-3-PO_4^{2-}) markedly attenuates CTII's disruptive effect, while two phosphates (PI-4,5-PO_4^{2-}) completely prevent membrane insertion, instead anchoring CTII at the membrane surface and promoting tighter lipid packing. If confirmed in future studies, these findings could inform the development of novel pharmaceuticals that protect cell membranes from attack by membrane-active protein toxins. Additionally, the findings of this study suggest that phosphorylated derivatives of phosphatidylinositol may protect nerve cell membranes from attack by amyloidogenic proteins. If future studies of amyloidogenic proteins interacting with membranes composed of PI and its phosphorylated derivatives yield results similar to those described here, phosphorylated derivatives of PI-and potentially other phospholipids-could be explored as novel pharmaceuticals for protecting brain cell membranes from aberrant amyloidogenic proteins such as beta-amyloid.

Acknowledgements

This study was supported from the start-up grant from the Chaoyang Kaiwen Academy (ESG) and in part by a pilot grant supported by the parent NIH grant UTGM148080 (RKD).

Conflict of Interest

The authors declare no conflict of interest.

Bibliography

1. A De Matteis and P De Camilli. "Phosphoinositides". *Biochimica et Biophysica Acta (BBA) - Lipids and Lipid Metabolism* 1851 (2015): 697-918.

2. MR Hokin and LE Hokin. "Enzyme secretion and the incorporation of P32 into phospholipids of pancreas slices". *Journal of Biological Chemistry* 203.2 (1953): 967-977.

3. LE Hokin and MR Hokin. "Effects of acetylcholine on the turnover of phosphoryl units in individual phospholipids of pancreas slices and brain cortex slices". *Biochimica et Biophysica Acta* 18.1 (1955): 102-110.

4. LE Hokin and MR Hokin. "Phosphoinositides and protein secretion in pancreas slices". *Journal of Biological Chemistry* 233.4 (1958): 805-810.

5. L Palamiuc., *et al*. "Phosphoinositides in autophagy: current roles and future insights". *FEBS Journal* 287.2 (2020): 222-238.

6. RC Wills and GRV Hammond. "PI(4,5)P_2: signaling the plasma membrane". *Biochemical Journal* 479.21 (2022): 2311-2325.

7. Y Atsuko "A molecular mechanism of phosphoinositides transport to the plasma membrane outer leaflet and its function in cancer progression". *Kaken* (2024).

8. K Ando., *et al*. "Dysregulation of phosphoinositide 5-phosphatases and phosphoinositides in Alzheimer's disease". *Frontiers in Neuroscience* 15 (2021): 614855.

9. B Cheng., *et al*. "Inhibiting toxic aggregation of amyloidogenic proteins: A therapeutic strategy for protein misfolding diseases". *Biochimica et Biophysica Acta* 1830.10 (2013): 4860-4871.

10. B Zhang., *et al*. "*Naja mossambica mossambica* cobra cardiotoxin targets mitochondria to disrupt mitochondrial membrane structure and function". *Toxins* 11.3 (2019): 152.

11. ES Gasanoff and RK Dagda. "Cobra venom cytotoxins as a tool for probing mechanisms of mitochondrial energetics and understanding mitochondrial membrane structure". *Toxins* 16.7 (2024): 287.

12. SE Gasanov., *et al*. "Snake venom cytotoxins, phospholipase A_2, and Zn-dependent metalloproteinases: Mechanisms of action and pharmacological relevance". *Journal of Clinical Toxicology* 4.1 (2014): 1000181.

13. SE Gasanov., *et al*. "*Naja naja oxiana* cobra venom cytotoxins CTI and CTII disrupt mitochondrial membrane integrity: Implications for basic three-fingered cytotoxins". *PLoS ONE* 10.6 (2015): e0129248.

14. SE Gasanov., *et al*. "Non-bilayer structures in mitochondrial membranes regulate ATP synthase activity". *Biochimica et Biophysica Acta* 1860.2 (2018): 586-599.

15. SE Gasanov, *et al*. "The possible role of nonbilayer structures in regulating ATP synthase activity in mitochondrial membranes". *Biophysics* 61.4 (2016): 596-600.

16. M Li and ES Gasanoff. "Cationic proteins rich in lysine residue trigger formation of non-bilayer lipid phases in model and biological membranes: Biophysical methods of study". *Journal of Membrane Biology* 256.4-6 (2023): 373-391.

17. I Ivanov. "Calorimetric methods of studying biopolymers and membrane systems". In: Chapter VA, Rubin (Edition) Modern Methods of Biophysical Investigations - a Practicum of Biophysics, Vyshaya Shkola, Moscow (1988): 203-216.

18. EV Grishin., *et al*. "The isolation and sequence determination of a cytotoxin from the Middle-Asian cobra *Naja naja oxiana*". *FEBS Letters* 48.2 (1974): 179-183.

19. O Trott and AJ Olson. "AutoDock Vina: improving the speed and accuracy of docking with a new scoring function, efficient optimization, and multithreading". *Journal of Computational Chemistry* 31.2 (2010): 455-461.

20. ThermoFisher Scientific. Safety data sheet. Product Name Methanol (2025).

21. ThermoFisher Scientific. Safety data sheet. Product Name Chloroform, stabilized with amylene (2025).

22. PV Dubovskii and YN Utkin. "Cobra cytotoxins: structural organization and antibacterial activity". *Acta Naturae* 6.3 (2014): 11-18.

23. https://cn.bing.com/images/search?view=detailV2&ccid=W%2FmjuAqg&id=B8C38FA7267513D520AC6463F6B0330312A69F3F&thid=OIP.W_mjuAqgsECrIhe5SxeYUwHaFj&mediaurl=https%3A%2F%2Fwww.researchgate.net%2Fprofile%2FTarik_Belhocine%2Fpublication%2F51980719%2Ffigure%2Ffig1%2FAS%3A202616735834112%401425319002126%2FPhospholipid-bilayer-composed-of-hydrophobic-non-polar-tails-and-hydrophilic-polar

24. TF Aripov., *et al*. "The influence of cytotoxins from Central Asian cobra venom and melittin from bee venom on the thermodynamic properties of phospholipid bilayer". *General Physiology and Biophysics* 6.4 (1987): 343-357.

Volume 14 Issue 3 March 2026